Modelling metallic discontinuities with the non-orthogonal finite difference time domain method

R. Nilavalan, I.J. Craddock and C.J. Railton

Abstract: Numerical electromagnetic models, such as the finite difference time domain (FDTD) method, have many applications. The authors focus on the non-orthogonal FDTD method, which offers an improved geometric flexibility compared to other standard techniques. Results from numerical electromagnetic analysis methods, such as the FDTD method, are often degraded by an error known as numerical dispersion. For metallic structures this dispersion error is often higher than expected from theoretical considerations. The source of this additional error is due to the reciprocal field interpolation scheme used in the non-orthogonal FDTD algorithm. The error is illustrated by means of a microstrip waveguide and a microstrip antenna. Techniques for reducing this error are evaluated; careful construction of the mesh at the metallic boundary being the most reliable solution.

1 Introduction

The finite difference time domain (FDTD) method has been widely used in the solution of electromagnetic problems. This method was originally put forward by Yee [1] and implemented in cartesian coordinates. However, if the structure being modelled does not align to the orthogonal cartesian grid, staircasing errors are introduced. To resolve this problem, a number of conformal mesh-based FDTD methods have been developed, such as contour path FDTD (CPFDTD) [2], non-orthogonal FDTD [3, 4] and the discrete surface integral (DSI) [5] method.

This particular contribution focuses on the non-orthogonal FDTD method. This method is based on a discretisation of Maxwell's curl equations in local curvilinear coordinates on a structured mesh employing covariant and contravariant field components. When the mesh is non-orthogonal, errors (notably dispersion and spurious reflection) arise which have been described in [6]. Importantly, however, at metallic boundaries the reciprocal interpolation scheme needed for stability introduces additional errors.

These additional errors have received little attention in the literature. [7] and [8] discuss the effect in terms of the error introduced in the resonant frequencies of simple closed cavities, as opposed to the microstrip structures considered herein, which shows some additional findings related to this problem. Analysis of this error based on a limited number of resonant frequencies will not show the true nature of these errors, since it is frequency dependent: as shown in this contribution. However, resonance in closed cavities involves wave propagation in many different directions and unless the mesh is carefully constructed, the error will be a combination of all these different effects. In [7], a non-orthogonal FDTD algorithm, different to the one analysed here was considered that has some late time stability problems. In [8], two approaches were suggested to reduce these errors, in the first approach a locally asymmetric scheme was proposed and in the second a more physical approach where the actual field behaviour near metal boundaries was employed to compensate the errors. The first approach was considered and found to be less than ideal in practice and an alternative technique (which was also considered in [7]) is considered. The second approach mentioned in [8] is outside the scope of this contribution.

IEE Proceedings online no. 20040764
doi:10.1049/ip-map:20040764
Paper first received 18th December 2003 and in revised form 18th May 2004. Originally published online: 21st July 2004

The authors are with the Centre for Communications Research, Faculty of Engineering, University of Bristol, Bristol BS8 1UB, UK

2 Modelling metal boundaries with non-orthogonal coordinates

Non-orthogonal FDTD is formulated on a structured grid, described by a local non-orthogonal coordinate system, which is characterised by covariant unit vectors $\boldsymbol{U}_1$, $\boldsymbol{U}_2$ and $\boldsymbol{U}_3$ (tangential to the unit cell edges) as shown by Fig. 1, and contravariant unit vectors $\boldsymbol{U}^1$, $\boldsymbol{U}^2$ and $\boldsymbol{U}^3$ (lying normal to the cell faces).

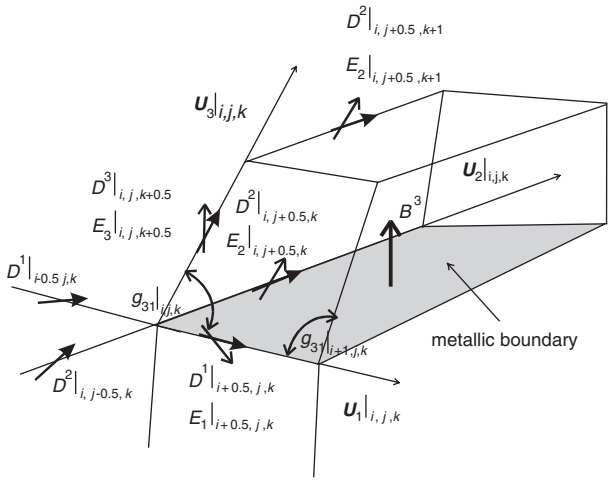

Fig. 1 *Location of a metallic boundary in a unit cell*

The non-orthogonal algorithm may be described by a system of matrix-vector equations [9], an iteration step (where new values of the contravariant fields are calculated):

$$\begin{aligned}\frac{\boldsymbol{D}^{n+1}-\boldsymbol{D}^{n}}{\Delta t}&=\boldsymbol{C}_h\boldsymbol{H}^{n+1/2}\\ -\frac{\boldsymbol{B}^{n+1/2}-\boldsymbol{B}^{n-1/2}}{\Delta t}&=\boldsymbol{C}_e\boldsymbol{E}^{n}\end{aligned}\tag{1}$$

and an interpolation step (yielding covariant components):

$$E_i=\sum_j\frac{\boldsymbol{U}_i\cdot\boldsymbol{U}_j}{\varepsilon\sqrt{g}}D^j\Rightarrow\boldsymbol{E}=\boldsymbol{M}_\varepsilon\boldsymbol{D}\tag{2}$$

and, similarly:

$$\boldsymbol{H}=\boldsymbol{M}_\mu\boldsymbol{B}\tag{3}$$

where $\boldsymbol{E}$ and $\boldsymbol{H}$ are vectors consisting of all the covariant field values in the algorithm, $\boldsymbol{B}$ and $\boldsymbol{D}$ are the contravariant components and $\boldsymbol{C}_e$ and $\boldsymbol{C}_h$ are matrices that implement the curl operation. $\boldsymbol{M}_\varepsilon$ and $\boldsymbol{M}_\mu$ are matrices that describe both material properties and the interpolation that yields the necessary covariant components. $\sqrt{g}$ represents the volume of the cell.

Considering the covariant component $E_1|_{i+0.5,j,k}$ in Fig. 1, the interpolation step (2), yields:

$$\begin{aligned}E_1|_{i+0.5,j,k}=&\frac{\boldsymbol{U}_1|_{i,j,k}\cdot\boldsymbol{U}_1|_{i,j,k}}{\varepsilon\sqrt{g}}D^1|_{i+0.5,j,k}\\&+\left\{\frac{\boldsymbol{U}_1|_{i,j,k}\cdot\boldsymbol{U}_3|_{i,j,k}}{4\varepsilon\sqrt{g}}D^3|_{i,j,k+0.5}\right.\\&+\frac{\boldsymbol{U}_1|_{i,j,k}\cdot\boldsymbol{U}_3|_{i+1,j,k}}{4\varepsilon\sqrt{g}}D^3|_{i+1,j,k+0.5}\\&+\frac{\boldsymbol{U}_1|_{i,j,k}\cdot\boldsymbol{U}_3|_{i,j,k-1}}{4\varepsilon\sqrt{g}}D^3|_{i,j,k-0.5}\\&+\frac{\boldsymbol{U}_1|_{i,j,k}\cdot\boldsymbol{U}_3|_{i+1,j,k-1}}{4\varepsilon\sqrt{g}}D^3|_{i+1,j,k-0.5}\\&+\frac{\boldsymbol{U}_1|_{i,j,k}\cdot\boldsymbol{U}_2|_{i,j,k}}{4\varepsilon\sqrt{g}}D^2|_{i,j+0.5,k}\\&+\frac{\boldsymbol{U}_1|_{i,j,k}\cdot\boldsymbol{U}_2|_{i,j-1,k}}{4\varepsilon\sqrt{g}}D^2|_{i,j-0.5,k}\\&+\frac{\boldsymbol{U}_1|_{i,j,k}\cdot\boldsymbol{U}_2|_{i+1,j,k}}{4\varepsilon\sqrt{g}}D^2|_{i+1,j+0.5,k}\\&\left.+\frac{\boldsymbol{U}_1|_{i,j,k}\cdot\boldsymbol{U}_2|_{i+1,j-1,k}}{4\varepsilon\sqrt{g}}D^2|_{i+1,j-0.5,k}\right\}\end{aligned}\tag{4}$$

where, g must be calculated using the local unit vectors associated with that perticular component. i.e. in

$$\frac{\boldsymbol{U}_1|_{i,j,k}\cdot\boldsymbol{U}_3|_{i,j,k}}{4\varepsilon\sqrt{g}}D^3|_{i,j,k+0.5}$$

g must be calculated using $\boldsymbol{U}_1|_{i,j,k}$ and $\boldsymbol{U}_3|_{i,j,k}$.

Whereas for $E_3|_{i,j,k+0.5}$, the interpolation gives:

$$\begin{aligned}E_3|_{i,j,k+0.5}=&\frac{\boldsymbol{U}_3|_{i,j,k}\cdot\boldsymbol{U}_3|_{i,j,k}}{\varepsilon\sqrt{g}}D^3|_{i,j,k+0.5}\\&+\left\{\frac{\boldsymbol{U}_3|_{i,j,k}\cdot\boldsymbol{U}_1|_{i,j,k}}{4\varepsilon\sqrt{g}}D^1|_{i+0.5,j,k}\right.\\&+\frac{\boldsymbol{U}_3|_{i,j,k}\cdot\boldsymbol{U}_1|_{i,j,k+1}}{4\varepsilon\sqrt{g}}D^1|_{i+0.5,j,k+1}\\&+\frac{\boldsymbol{U}_3|_{i,j,k}\cdot\boldsymbol{U}_1|_{i-1,j,k}}{4\varepsilon\sqrt{g}}D^1|_{i-0.5,j,k}\\&+\frac{\boldsymbol{U}_3|_{i,j,k}\cdot\boldsymbol{U}_1|_{i-1,j,k+1}}{4\varepsilon\sqrt{g}}D^1|_{i-0.5,j,k+1}\\&+\frac{\boldsymbol{U}_3|_{i,j,k}\cdot\boldsymbol{U}_2|_{i,j,k}}{4\varepsilon\sqrt{g}}D^2|_{i,j+0.5,k}\\&+\frac{\boldsymbol{U}_3|_{i,j,k}\cdot\boldsymbol{U}_2|_{i,j,k+1}}{4\varepsilon\sqrt{g}}D^2|_{i,j+0.5,k+1}\\&+\frac{\boldsymbol{U}_3|_{i,j,k}\cdot\boldsymbol{U}_2|_{i,j-1,k}}{4\varepsilon\sqrt{g}}D^2|_{i,j-0.5,k}\\&\left.+\frac{\boldsymbol{U}_3|_{i,j,k}\cdot\boldsymbol{U}_2|_{i,j-1,k+1}}{4\varepsilon\sqrt{g}}D^2|_{i,j-0.5,k+1}\right\}\end{aligned}\tag{5}$$

For stability [9] the material matrices $\boldsymbol{M}_\varepsilon$ and $\boldsymbol{M}_\mu$ must be symmetric, this is achieved as a result of the coupling between components $E_1|_{i+0.5,j,k}$ and $E_3|_{i,j,k+0.5}$, given by (4) and (5), being reciprocal, since:

$$\frac{\boldsymbol{U}_3|_{i,j,k}\cdot\boldsymbol{U}_1|_{i,j,k}}{4\varepsilon\sqrt{g}}=\frac{\boldsymbol{U}_1|_{i,j,k}\cdot\boldsymbol{U}_3|_{i,j,k}}{4\varepsilon\sqrt{g}}$$

However, at a metallic boundary, such as that shown in Fig. 1, the tangential electric field $E_1|_{i+0.5,j,k}$ must be zero, and hence the contribution to this component from $E_3|_{i,j,k+0.5}$ ($D^3|_{i,j,k+0.5}$) in (4), must be set to zero. However, as a necessary consequence of reciprocity, the contribution from $E_1|_{i+0.5,j,k}$ ($D^1|_{i+0.5,j,k}$) to $E_3|_{i,j,k+0.5}$ in (5) must also then be zero (if this is ignored, instability will result).

In effect therefore it appears to the model as if $\boldsymbol{U}_3|_{i,j,k}\cdot\boldsymbol{U}_1|_{i,j,k}=0$, which is not true unless the mesh is orthogonal at the boundary. This is an undesirable approximation, which gives rise to additional error in non-orthogonal FDTD; this error is examined in the following Section.

Schumann *et al.* [8] suggested that these errors in resonant cavity problems can be compensated by simply increasing the weight of the remaining terms in the interpolation formula, (5), while maintaing the symmetry criteria. i.e. the:

$$\frac{\boldsymbol{U}_3|_{i,j,k}\cdot\boldsymbol{U}_1|_{i,j,k+1}}{4\varepsilon\sqrt{g}}\quad\frac{\boldsymbol{U}_3|_{i,j,k}\cdot\boldsymbol{U}_1|_{i-1,j,k}}{4\varepsilon\sqrt{g}}\quad\frac{\boldsymbol{U}_3|_{i,j,k}\cdot\boldsymbol{U}_1|_{i-1,j,k+1}}{4\varepsilon\sqrt{g}}$$

and $\dfrac{\boldsymbol{U}_3|\cdot\boldsymbol{U}_2|}{4\varepsilon\sqrt{g}}$

terms in (5) can be multiplied by an appropriate factor and the same value is then used in the calculation of the fields such as $E_2|_{ij+0.5,k+1}$ to ensure stability. This muliplying factor can be determined by considering the number of field vectors that are available for interpolation. In general four electric fields are considered for interpolation for a single field, but due to the stability criteria at the metal boundaries the contribution from some electric fields is neglected, hence this factor is determined depending on the available fields (i.e. if three fields are available then 4/3, but it can also be

further improved for better results). This suggestion is considered in the following Section, along with an alternative technique.

3 Numerical Results

3.1 Microstrip line

Figure 2 shows an air-spaced (non-dispersive) microstrip line which is used here to demonstrate the metallic boundary effect through an analysis of the numerical dispersion in the model [6].

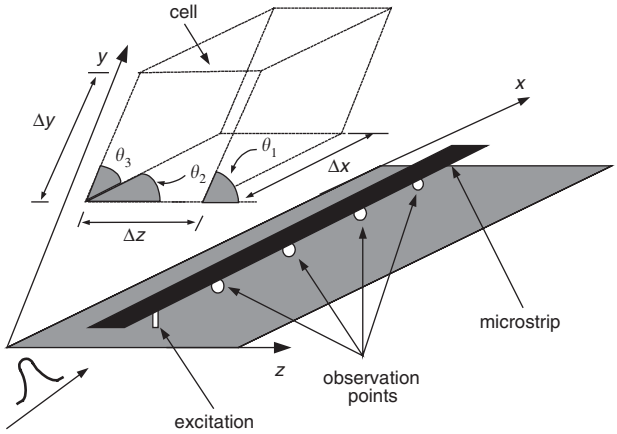

Fig. 2 *Microstrip line and description of skewed cells*

A Gaussian pulse with a 300 ps width was used to excite the problem and the electric fields were observed at four different locations. The microstrip line was made sufficiently long to avoid any problems from absorbing boundary conditions [10]. Mur's first-order conditions were employed with the following provisos to avoid complexities arising due to non-orthogonal unit cells: (i) orthogonal cells are employed at the absorbing boundaries parallel to the microstrip line, and (ii) the interpolation step is ignored at the absorbing boundaries truncating the microstrip line. The problem space was uniformly discretised into $140 \times 25 \times 20$ unit cells each with a dimension of 6.5 mm in the longitudinal direction. As shown in Fig. 2, the unit cells were distorted with either two or three angles of skew (θ_1, θ_2 and θ_3), which in all cases were 60°. The problem space was limited by using absorbing boundaries and an electric wall to represent the ground plane.

The dispersion suffered by the pulse as it propagates through the model was calculated as described in [6], and compared with meshes that incorporated orthogonal grids in the vicinity of the metallic surfaces (i.e. the microstrip and the ground plane, Figs. 3 and 4) and with the theoretical 60° dispersion curve from the numerical dispersion relation (NDR) [11]. The incorporation of orthogonal grids at the metallic boundaries did not introduce any instabilities, since the stability criteria for the non-orthogonal FDTD method is still maintained. The dispersion from the modified-weighting technique [8] is also considered (with multiplying factors of 4/3.5 and 4/3.0). Figures 5 and 6 show the normalised wave numbers for meshes with two and three equal angles of skew respectively [6].

These results clearly show that the non-orthogonal meshes introduce errors leading to additional dispersion over that expected from the NDR, and it can be seen that these errors persist even when the mesh size is reduced to a very small fraction of a wavelength. It is believed that this additional error is due to problems at the metallic

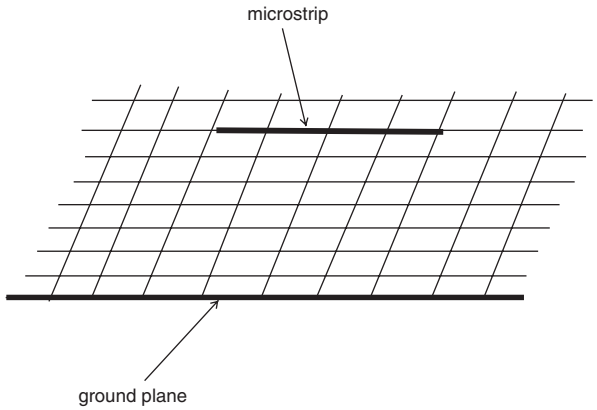

Fig. 3 *Non-orthogonal mesh*

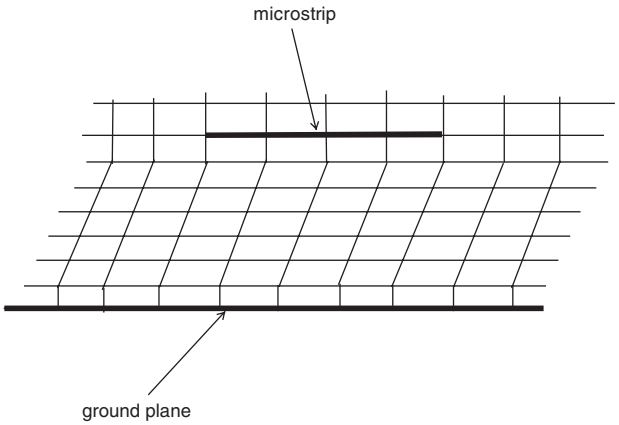

Fig. 4 *Locally orthgonal mesh at metal surfaces*

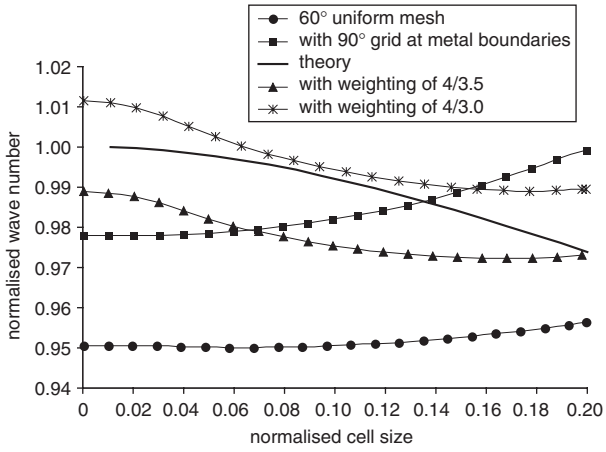

Fig. 5 *Dispersive behaviour with two equal skew angles*

boundaries described in the preceeding Section; evidence for this is that if the mesh is forced to be orthogonal or if modified weightings [8] are incorporated at the metallic surface, then the dispersion error is dramatically reduced. Since the same conditions (i.e. mesh size, probe location, and strip width) were maintained with these numerical experiments, this clearly demonstrates the effects of having non-orthogonal meshes at metallic surfaces.

3.2 Microstrip Patch Antenna

Figure 7 shows a second test structure, this time an air-spaced microstrip patch antenna (50×40 mm, lying 3.2 mm above the ground plane); a dielectric substrate was not included in this structure in order to simplify the problem and to separate the errors due to the metallic boundary. As

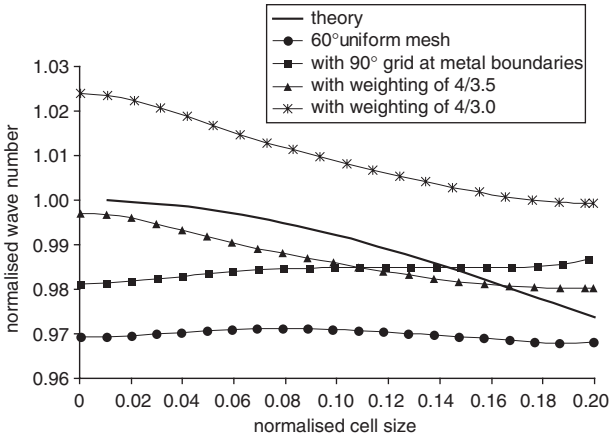

Fig. 6 *Dispersive behaviour with three equal skew angles*

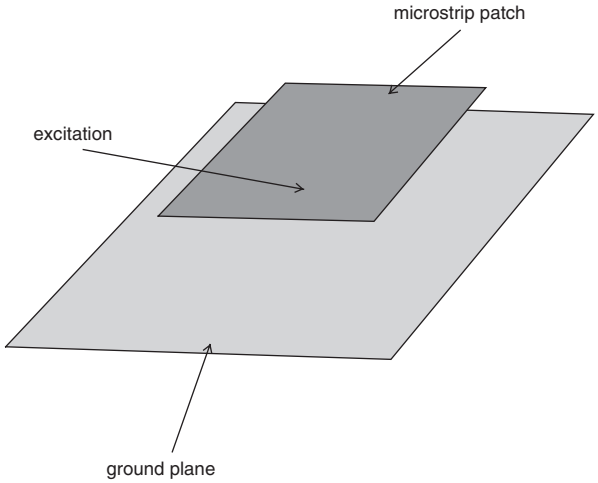

Fig. 7 *Air-spaced microstrip patch antenna*

before, Mur's first-order absorbing condition was employed to limit the problem space. For simplicity, a feed is not included, the fields being excited and recorded directly on the antenna. Analyses were conducted with four different test mesh configurations for six numerical experiments:

- Mesh 1: Fine orthogonal mesh ($42 \times 34 \times 8$ cells across the patch), which provides a reference result.
- Mesh 2: Orthogonal mesh ($20 \times 16 \times 5$ cells across the patch).
- Mesh 3: Uniformly skewed mesh with one angle of skew (a worst case of 45°) but otherwise with the same cell sizes and number of cells as mesh 2 (Fig. 3).
- Mesh 4: As mesh 3 but with orthogonal cells at the metallic surfaces (Fig. 4).
- Correction 1: As mesh 3 but using a modified weighting factor of 4/3.5.
- Correction 2: As mesh 3 but using a modified weighting factor of 4/3.75.

Mesh 1 was used to obtain an accurate frequency response of the patch whereas meshes 2, 3 and 4 were chosen to give results from different mesh configurations. It should be noted that meshes 2, 3 and 4 were carefully chosen so that they had similar cell sizes in all directions.

Figure 8 shows a discrete Fourier transform (DFT) of the response of the patch. As expected, of the two non-orthogonal meshes, mesh 4 outperforms mesh 3, very closely following the fine orthogonal mesh result, since it

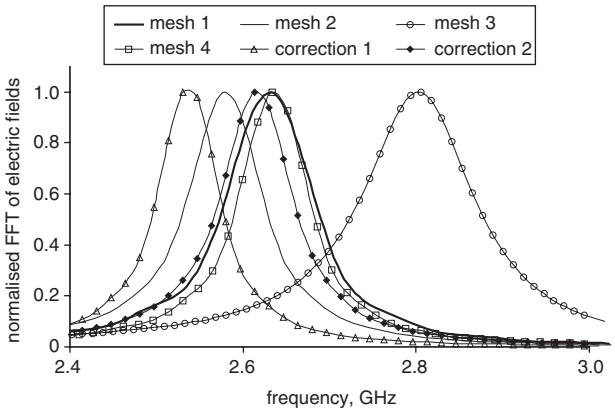

Fig. 8 *Frequency response of the patch*

eliminates the problems with modelling metallic boundaries. Applying the modified weighting technique only produced good results with a multiplying factor of 4/3.75.

It should be noted that mesh 4 even performs slightly better than the orthogonal mesh with the same density (mesh 2). This is probably because mesh 4 has a mixture of orthogonal cells at the metal (in which the fields travel slightly too slowly [5]) and skewed cells (in which the fields travel too fast); these dispersion errors oppose each other, and so may well cancel each other to some extent. On the other hand the entirely orthogonal mesh (mesh 2) gives a lower estimated frequency due to the speed of propagation being everywhere too slow.

The numerical results from the two test structures in this Section confirm that significant dispersive errors are indeed introduced if, at a metallic boundaries on a non-orthogonal mesh, it is assumed that the covariant tangential electric field components and the couplings from their contravariant components are zero (e.g. $\boldsymbol{U}_3|_{i,j,k} \cdot \boldsymbol{U}_1|_{i,j,k} = 0$). As can be seen in Figs 5 and 6, the normalised wave numbers remain around 0.95 and 0.97 respectively even for very fine meshes.

Applying modified weights in the interpolation, as suggested in [8], generally improved the results, but the correct choice of interpolation weights seems to be rather arbitrary, and strongly dependent on the problem being considered (ranging from 4/3.0 to 4/3.75 in the cases considered herein). The alternative, suggested herein, is to employ orthogonal meshes at metal surfaces; this gives much improved results in all cases (even though it results in a more distorted mesh).

4 Conclusions

The modelling of metallic boundaries using a non-orthogonal FDTD method has been presented. The difficulties in representing metallic boundaries have been described and the errors associated with the modelling of metal objects have been illustrated by means of test cases including a microstrip line and a patch antenna.

The modelling of metal surfaces using non-orthogonal meshes by assuming that the covariant tangential electric field components, and the coupling from their contravariant components, is zero, results in significant errors leading to numerical dispersion. This effect has been clarified by comparing the results with the theoretical estimations and with meshes where the mesh reverts to an orthogonal configuration at the boundaries of metal structures.

The dispersive behaviour was further analysed through the analysis of a patch antenna. As expected, a mesh which

employs orthogonal cells in the vicinity of the metal surfaces gave a much improved estimation of the resonant frequency. Applying modified weights in the non-orthogonal algorithm's interpolation process also yielded improved results but the choice of weights is problem dependent and it seems unlikely that the correct values can be determined *a priori*.

In conclusion, while non-orthogonal meshes offer a solution to staircasing problems in FDTD, the mesh should be as close to orthogonal as possible at any metallic surfaces unless suitable correction techniques are employed.

5 Acknowledgments

The authors would like to thank Professors McGeehan and Bull for provision of facilities at the University of Bristol, and EPSRC for supporting this work.

6 References

1 Yee, K.S.: 'Numerical solutions of initial boundary value problems involving Maxwell's equations in isotropic media', *IEEE Trans. Antennas Propag.*, 1966, **14**, pp. 302–307

2 Jurgens, T.G., Taflove, A., Umashankar, K.R., and Moore, T.G.: 'Finite difference time domain modelling of curved surfaces', *IEEE Trans. Antennas Propag.*, 1992, **40**, pp. 357–366

3 Holland, R.: 'Finite-difference solution of Maxwell's equations in generalized nonorthogonal coordinates', *IEEE Trans. Nucl. Sci.*, 1983, **30**, pp. 4586–4591

4 Hao, Y., and Railton, C.J.: 'Analysing electromagnetic structures with curved boundaries on cartesian FDTD meshes', *IEEE Trans. Microw. Theory Tech.*, 1998, **46**, pp. 82–88

5 Gedney, S., Lansing, F.S., and Rascoe, D.L.: 'Full wave analysis of microwave monolithic circuit devices using a generalised Yee-algorithm based on an unstructured grid', *IEEE Trans. Microw. Theory Tech.*, 1996, **44**, pp. 1393–1400

6 Nilavalan, R., Craddock, I.J., and Railton, C.J.: 'Quantifying numerical dispersion in non-orthogonal FDTD meshes', *IEE Proc., Microw. Antennas Propag.*, 2002, **149**, pp. 23–27

7 Zhao, L., Tong, L.S., and Carter, R.G.: 'The influence of boundary conditions on resonant frequencies of cavities in 3-D FDTD algorithm using non-orthogonal co-ordinates', *IEEE Trans. Magn.*, 1994, **30**, pp. 3570–3573

8 Schumann, R., Hilgner, M., and Weiland, T.: 'Convergence properties of the nonorthogonal FDTD algorithm'. Proc. 2000 USNC/URSI National Radio Science Meeting, Salt Lake City, UT, USA, p. 22

9 Schumann, R., and Weiland, T.: 'Stability of the FDTD algorithm on non-orthogonal grids related to the spatial interpolation scheme', *IEEE Trans. Magn.*, 1998, **34**, pp. 2751–2754

10 Mur, G.: 'Absorbing boundary conditions for the finite difference approximation of the time domain electromagnetic-field equations', *IEEE Trans. Electromagn. Compat.*, 1981, **23**, pp. 377–382

11 Shi, H., and Drewniak, J.L.: 'Dispersion comparison for DSI- and tensor-based non-orthogonal FDTD', *IEEE Microw. Guid. Wave Lett.*, 1996, **6**, pp. 193–195